Journal of Climate

Necessary Conditions for Tropical Cyclone Rapid Intensification as Derived from 11 Years of TRMM Data

--Manuscript Draft--

Manuscript Number:	JCLI-D-12-00432
Full Title:	Necessary Conditions for Tropical Cyclone Rapid Intensification as Derived from 11 Years of TRMM Data
Article Type:	Article
Abstract:	Convective and rainfall properties of tropical cyclones (TCs) are statistically quantified for different TC intensity change categories by using Tropical Rainfall Measuring Mission (TRMM) data from December 1997 to December 2008. Four 24-h future intensity change categories are defined: rapidly intensifying (RI), slowly intensifying, neutral, and weakening. Maximum convective intensity in the inner core is not necessarily more intense prior to undergoing an RI episode than a slowly intensifying, neutral, or weakening episode. Instead, a minimum threshold of convective intensity, raining area, and total volumetric rain in the inner core has to be reached before a storm undergoes RI. The following necessary conditions for RI are found in the inner core: maximum near surface radar reflectivity > 40 dBZ, maximum 20 (30, 40) dBZ echo height > 8 (6, 4) km, minimum 85 (37) GHz polarization corrected brightness temperature (PCT) < 235 (275) K, minimum 10.8 μm brightness temperature < 220 K, total raining area > 3,000 km2, and total volumetric rain > 5,000 mm h-1 km2. It is also found that total lightning activities in the inner core (outer rainband) have a negative (positive) relationship with storm intensification.

Necessary Conditions for Tropical Cyclone Rapid Intensification as Derived from 11 Years of TRMM Data

Haiyan Jiang*

Department of Earth & Environment, Florida International University, Miami, Florida

Ellen M. Ramirez

Department of Atmospheric Sciences, University of Utah, Salt Lake City, Utah

Submitted to JCLI: July 12, 2012

*Corresponding author address: Dr. Haiyan Jiang, Department of Earth & Environment, Florida International University, 11200 SW. 8th Street, PC-342B, Miami FL. Phone: 305-348-2984; Fax: 305-348-3877; Email: haiyan.jiang@fiu.edu

Abstract

Convective and rainfall properties of tropical cyclones (TCs) are statistically quantified for different TC intensity change categories by using Tropical Rainfall Measuring Mission (TRMM) data from December 1997 to December 2008. Four 24-h future intensity change categories are defined: rapidly intensifying (RI), slowly intensifying, neutral, and weakening. Maximum convective intensity in the inner core is not necessarily more intense prior to undergoing an RI episode than a slowly intensifying, neutral, or weakening episode. Instead, a minimum threshold of convective intensity, raining area, and total volumetric rain in the inner core has to be reached before a storm undergoes RI. The following necessary conditions for RI are found in the inner core: maximum near surface radar reflectivity > 40 dBZ, maximum 20 (30, 40) dBZ echo height > 8 (6, 4) km, minimum 85 (37) GHz polarization corrected brightness temperature (PCT) < 235 (275) K, minimum 10.8 μm brightness temperature < 220 K, total raining area > 3,000 km^2, and total volumetric rain > 5,000 mm h^{-1} km^2. It is also found that total lightning activities in the inner core (outer rainband) have a negative (positive) relationship with storm intensification.

1. Introduction

Understanding and predicting intensity changes, especially rapid intensification (RI), of tropical cyclones (TCs) require some understanding of not only the large-scale environment condition, but also the convective and precipitation properties of the storm. It has been well agreed that the necessary environmental conditions of TC intensification and RI include warmer sea surface temperature, higher low to middle level moisture, and lower vertical wind shear (Merrill 1988, Kaplan et al. 2010). As for the rate of TC intensity change, Hendricks et al. (2010) found that it is only weakly dependent on environmental conditions. Therefore, they argued that RI is more likely controlled by TC internal processes.

Convective and precipitation properties in the inner core are closely related to the latent heating release which is crucial of storm development. Previous studies have shown some relationships between TC intensification and inner core rainfall and convective properties such as rain rate (Rao and MacAuthur 1994), convective bursts (Steranka et al. 1986), ice scattering signatures (Cecil and Zipser 1999), hot towers (Hendricks et al. 2004; Kelley et al. 2004, 2005; Montgomery et al. 2006) and lightning activities (Lyons and Keen 1994, Molinari et al. 1999). An asymmetric paradigm of TC intensification has been proposed by Montgomery and Smith (2011) in summarizing previous studies recognizing the importance of "vortical hot towers" (i.e. rotating deep convection).

Fewer studies are documented with a focus on RI. Jiang (2012) compared the convective properties, i.e., radar reflectivity profiles, infrared (IR) cloud top temperature, and passive microwave ice scattering signature in the inner core for 24-h future rapidly intensifying, slowly intensifying, neutral, slowly weakening and rapidly weakening storms. The hypothesis was that extremely intense convection, such as hot towers in the inner core is the sufficient condition for

RI. She found that the minimum infrared (IR) brightness temperature, upper-level maximum radar reflectivity, and maximum 20 dBZ radar echo height in the inner core are best associated with the rate of TC intensity change among all the convective parameters examined. She also found that the probability of RI increases slightly when these parameters show stronger than average convective intensity in the inner core. However, Jiang (2012) argued that hot towers are neither necessary nor sufficient condition for RI.

Kieper and Jiang (2012) demonstrated that a precipitative ring pattern around the TC center is a very good predictor of RI. This seems support the symmetric intensification mechanism as proposed by many theoretical studies (Ooyama 1969, Smith 1981, Shapiro and Willoughby 1982, Nolan et al. 2007). Opposite to the asymmetric paradigm of TC intensification, the symmetric mechanism emphasizes that a TC intensifies through an axisymmetric heating mechanism, where the symmetric secondary circulation draws air from outer radii above the boundary layer while conserving absolute angular momentum. Kieper and Jiang (2012)'s results also suggest that some necessary conditions might exist for RI in terms of the size of raining area and total precipitation in the inner core.

DeMaria et al. (2012) examined the relationships between lightning activity and RI using 6 years of World Wide Lightning Location Network (WWLLN) data for Atlantic and eastern North Pacific TCs. Surprisingly, they found that rapidly weakening TCs have larger lightning density in the inner core (0-100 km) than RI storms, and the lightning density in the rain band regions (200-300 km) is higher for storms that rapidly intensified in the following 24 h. However, as indicated by DeMaria et al. (2012), the fixed radius distance used in their study caused some structure loss, especially when studying a large sample of TCs with various storm sizes, e.g., Atlantic vs. north Western Pacific storms. A question from here is whether their results hold true when using a more appropriate method to separate inner core and rain band regions.

Jiang et al. (2012, hereafter JRC) document the distributions of convective and rainfall properties in TC inner cores and rainbands in the dataset used here. To account for varying TC sizes, JRC manually separated inner core (IC), inner rainband (IB), and outer rainband (OB) regions for all the Tropical Rainfall Measuring Mission (TRMM) satellite TC overpasses during December 1997 through December 2008. The separation is based on convective structure, such as the horizontal fields of radar reflectivity and passive microwave ice scattering. In this study, the primary interest is on the relationship between both convective and rainfall properties in the inner core and TC intensity changes, especially rapid intensification. A particular purpose is to see if there are necessary conditions for RI in terms of rainfall and convective properties in the inner core. If so, what are they? The parameters to be examined include radar reflectivity, passive microwave brightness temperature at 85 and 37 GHz, IR cloud top brightness temperature, lightning flash counts, raining area, rain rate, and total volumetric rain. The lightning results will be compared with DeMaria et al. (2012). The organization of the remainder of the paper is as follow. The data and methodology are briefly described on section 2. The distributions of these convective and rainfall properties as a function of different TC intensity change categories are presented in section 3. A series of necessary conditions for RI in terms of these inner core properties are also presented in section 3. Discussions are provided in section 4, and conclusions in section 5.

2. Data and Methodology

2.1. TRMM TC data

The same dataset from the TRMM Tropical Cyclone Precipitation Feature (TCPF) database (Jiang et al. 2011) is used in this study as in JRC. It includes global TCs that were observed by the TRMM satellite during December 1997 through December 2008. The categorization of inner core (IC), inner rainband (IB), and outer rainband (OB) regions in TRMM TC overpasses is described in section 2.1 of JRC. Same as JRC, two sets of samples are used in this study in order to maximize the sample size and use the unique 3-D observations from the radar: one is from TRMM overpasses within the TRMM Microwave Imager (TMI) swath, and the other is within the Precipitation Radar (PR) swath. The selection of TRMM overpasses is described in section 2.3 of JRC. In this study, TRMM derived parameters selected for the analysis of TC samples in the TMI swath include minimum 85/37 GHz polarization corrected brightness temperatures (PCTs, Spencer et al. 1989 and Cecil et al. 2002), minimum 11 μm brightness temperature (T_{B11}), percentage of pixels with 85 GHz PCT < 250 and 225 K, 2A12 (Kummerow et al. 1996) conditionally mean rain rate, raining area, and total volumetric rain, and lightning flash counts. T_{B11} is observed by the TRMM Visible and Infrared Scanner (VIRS), and lightning flash counts are observed by Lightning Imaging Sensor (LIS) on TRMM. All other parameters are observed by the TMI. The swath widths of VIRS and LIS are similar to that of TMI, while the PR has a much narrower swath. Parameters selected for the analysis of samples in the PR swath include vertical profile of maximum radar reflectivity, maximum near surface reflectivity, maximum height of 20, 30, and 40 dBZ radar echo, 2A25 (Iguchi et al. 2000) conditionally mean rain rate, raining area, and total volumetric rain. All these parameters are observed by the PR. Section 2.4 of JRC provided a review of the physical meanings of these parameters and how they are referred as convective and rainfall proxies.

JRC compared the convective and rainfall properties among IC, IB, and OB regions in terms of large precipitation features. However, in this study each TRMM overpass, i.e., each storm is assigned a single value of rainfall and convective parameters for IC, IB, and OB regions, respectively. Since multiple features usually exist in the IC, IB, or OB region of one TC, we consider this storm-based approach is more appropriate for studying TC intensity changes. The number of TMI (PR) TC overpasses used in this study is 2712 (1100). The geographic distributions of these overpasses are given in Fig. 1. For parameters other than lightning flashes, only the inner core region is examined for the relationships with TC intensity changes. For lightning activities, both inner and rainbands are investigated to compare with the results of DeMaria et al. (2012).

2.2. Selection of TC intensity change categories

The TCPF database includes all intensity stages of TCs that reached tropical storm intensity level or above at least once in their lifetime. Therefore, each individual TRMM overpass included here could be at either tropical depression, tropical storm, or hurricane stage. The 24-h future storm intensity and intensity change corresponding to each overpass are interpolated from the 6-h best track data from the National Hurricane Center (NHC) for TCs in the North Atlantic and Eastern North Pacific basins and Joint Typhoon Warning Center (JTWC) for TCs in other basins. The TMI and PR swath samples are separated in four intensity change categories: rapidly intensifying (RI), slowly intensifying (SI), neutral (N), and weakening (W). Table 1 lists the four intensity change categories, along with the range and sample size. The threshold for each category is defined by following Jiang (2012).

Table 2 shows the distribution of the different intensity change samples as a function of the initial TC intensity. For both TMI and PR swath samples, storms that are initially of tropical storm intensity account for the largest percentage of RI cases while category 1-2 hurricanes contribute the next largest percentage. Both tropical depressions and tropical storms account for a larger percentage of slowly intensifying cases, while category 1-2 hurricanes account for the most of weakening cases. In terms of different TC-prone basins (table 3), RI cases are the most in the northwest Pacific basin, and the least in the north Indian Ocean basin. Note that the distribution as a function of different basin is similar for different intensity change categories.

3. Results

3.1 TMI and VIRS: brightness temperatures and 2A12 rainfall

TRMM observations within the TMI swath are used in this section to compare convective and rainfall characteristics in the inner core region for different intensity change categories. The cumulative distribution functions (CDFs) of the minimum 37 GHz and 85 GHz PCTs and minimum IR T_{B11} in the inner core for storms in different intensity change stages are presented in Fig. 2. As described in JRC, low values of 85 and 37 GHz PCT tend to indicate strong ice scattering signatures, and low values of IR T_{B11} indicate higher cloud tops. Therefore, all these parameters are used here as convective proxies. It is seen from Fig. 2 that at weaker convective spectrum, i.e., minimum 85 GHz PCT > ~150 K, minimum 37 GHz PCT > ~250 K, and minimum T_{B11} > 180-185 K, RI storms have stronger ice scattering signature and higher cloud top in the inner core than storms in other three intensity change categories, and slowly intensifying storms show much stronger convective intensity than neutral and weakening storms. However, at stronger convective spectrum, no significant difference among different intensity change categories is seen in the distributions of these convective parameters.

From Fig. 2, it is also interesting to observe that the maximum values (when the CDFs reach 100%) of the minimum 85 and 37 GHz PCT and IR T_{B11} for RI storms are much lower than those corresponding maximum values for storms in other intensity change categories. For example, the maximum value of minimum 85 GHz PCT (37 GHz PCT, IR T_{B11}) is about 235 K (275 K, 220 K) for RI storms, but reaches 280 K (280 K, 260-280 K) for storms in other intensity change stages. This indicates that a minimum threshold of convective intensity in the inner core has to be reached before a storm undergoes RI. This threshold can be deemed as necessary condition for RI. Therefore, the necessary conditions for RI derived from Fig. 2 are: 1) minimum 85 GHz PCT in the inner core is less than ~235 K (Fig. 2a), 2) minimum 37 GHz PCT in the inner core is less than ~275 K (Fig. 2b), and 3) minimum IR T_{B11} in the inner core is less than ~220 K (Fig. 2c). A threshold of 250 K for the 85 GHz PCT is considered as an indicator of moderate rain (Spencer et al. 1989, Mohr and Zipser 1996a, b), and 85 GHz PCT < 225 has been used as a criterion of convection (McGaughey et al. 1996, Mohr and Zipser 1996a, b). Therefore, the 235 K threshold of minimum 85 GHz PCT found here represents moderate to heavy rain. The traditional way to define deep convection from IR measurements is finding pixels with brightness temperatures colder than a given temperature threshold from IR images. This threshold could be 208 K (Mapes and Houze 1993, Hall and Vonder Haar 1999), 210 K (Zuidema 2003), 218 K (Machado et al. 1998), or cold point tropopause temperature (Gettelman et al. 2002). As shown in Gettelman et al. (2002), the cold point tropopause temperature over the Tropics varies between 180 K and 206 K. The base of tropopause region is about 215 K. Therefore, the 220 K of IR T_{B11} represents convective clouds that are close to, but not as deep as overshooting convection (i.e., hot towers).

Minimum brightness temperatures are extreme values which represent just one pixel in the inner core. The percentage of area satisfying a given PCT threshold is perhaps a more appropriate convective proxy. Fig. 3a indicates that the inner core of RI storms contain a larger percentage of area with 85 GHz PCT < 250 K (moderate rain), followed by slowly intensifying, weakening, and neutral storms. This is also generally true for percentage of area with 85 GHz PCT < 225 K (convection, Fig. 3b). However, the inner core of RI storms has the least percentage of pixels with 85 GHz PCT < 150 K (Fig. 3c), which represents very strong convection.

Fig. 4 shows the CDFs of TMI 2A12 (Kummerow et a. 1996) raining area, volumetric rain, and conditionally mean rain rate in the inner core region for different intensity change storms. It is obvious that storms that will undergo RI always have larger raining area and total volumetric rain in the inner core region than storms that will slowly intensify, be neutral, or weaken. Note that the x-axis of Fig. 4a &b is in log scale, therefore the difference is large even for small spacing among the curves. Similar to what is found in Fig. 2, the necessary conditions for RI found from Fig. 4 are: 1) total raining area in the inner core region is greater than 3,000 km^2 (Fig. 4a), and 2) the total volumetric rain in the inner core is greater than 5,000 mm $h^{-1}km^2$ (Fig. 4b). However, although in the lower rain rate spectrum (< 7.5 mm h^{-1}) the CDFs in Fig. 4c show that RI storms have higher conditionally mean rain rate in the inner core than storm in other intensity change categories, in the higher rain rate spectrum (≥9.5 mm h^{-1}), RI storms have lower conditionally mean rain rate in the inner core. No necessary conditions for RI in terms of conditionally mean rain rate in the inner core are found.

3.2 PR: Vertical Profiles of Radar Reflectivity and 2A25 Rainfall

TRMM observations within the PR swath are used in this section to compare convective and rainfall characteristics in the inner core for different intensity change storms. Fig. 5 shows the contoured frequency by altitude diagrams (CFADs, Yuter and Houze 1995) of maximum radar reflectivity in the inner core of TCs in different intensity change stages. The distribution is highly concentrated around the median profile for storms that will undergo RI, while a wider distribution is seen for storms in other intensity change categories. From Fig. 6, no significant difference is seen in the top 10% of maximum radar reflectivity profiles among storms in different intensity change categories, except that the weakening storms seem have stronger reflectivities below the freezing level than RI storms. The main reason is that a large fraction of weakening storms has stronger initial intensity (i.e., 28% major hurricanes and 38% category 1-2 hurricanes, table 2). As shown in JRC, stronger TCs, especially major hurricanes, have much heavier near surface rain rate and lower-level reflectivities in the inner core, while extremely strong convection (indicated by strong ice scattering signature and upper-level radar reflectivity) is often seen in tropical storms and depressions. As seen in table 2, about 46% of RI storms are tropical storms and 17% of them are tropical depressions. The median profile of RI storms shows much higher reflectivities above 10 km than storms in other intensity change categories. The median height of maximum 20 dBZ echo reaches about 14.5 km for RI storms, while this value is only 12.5, 12, and 11 km for slowly intensifying, neutral, and weakening storms. The biggest difference among different intensity change categories is in the bottom 10% of inner core maximum reflectivity profiles. For RI storms, the bottom 10% profile is much stronger than that for other intensity change categories and is almost as strong as the median profiles of neutral and slowly intensifying storms. At near surface, the bottom 10% of maximum reflectivity in the inner core of RI storms is 46 dBZ, which is 8, 12, and 12 dBZ stronger than that of slowly intensifying, neutral, and weakening storms, respectively. The bottom 10% of maximum 20 dBZ echo height in the inner core of RI storms is 10 km, which is 2, 2, and 4 km higher than that of slowly intensifying, neutral, and weakening storms, respectively. Just like what is found in section 3.1, Fig. 5 and 6 indicate that necessary conditions, i.e. minimum thresholds of convective and rainfall intensities in the inner core have to be reached before a storm undergoes RI.

Fig. 7 is to find out these necessary conditions using radar derived parameters. The box and whisker plots in Fig. 7 represent the distributions of maximum near surface reflectivity, maximum heights of 20, 30, and 40 dBZ radar echo in the inner core. The top of the box represents the 75% percentile, the center line the median, and the bottom of the box the 25% percentile. The whiskers extend to minimum and maximum of the range and outliers are plotted individually with circles. The distributions are much narrower for RI storms than those for storms in other intensity change categories. For RI storms, the maximum near surface reflectivity in the inner core never go under 40 dBZ, and the maximum heights of 20, 30, and 40 dBZ radar echo in the inner core never go lower than 8, 6, and 4 km, respectively. These are the necessary conditions for RI.

Similar to the CDFs of TMI 2A12 rain area and volumetric rain shown in Fig. 4a and b, the CDFs of PR 2A25 (Iguchi et al. 2000) raining area and volumetric rain (Fig. 8a and b) in the inner core region show that RI storms always have larger raining area and total volumetric rain in the inner core region than storms that will slowly intensify, be neutral, or weaken. Even though differences exist between 2A12 (Fig. 4c) and 2A25 rain rates (Fig. 8c) due to the discrepancy inherent within the PR 2A25 and TMI 2A12 algorithms, similarities between Fig. 4 and Fig. 8 are obvious. First of all, the necessary conditions for RI found from 2A25 raining area and total volumetric rain are the same as found from the 2A12 retrievals, which are: 1) total 2A25 raining area in the inner core region is greater than 3,000 km^2 (Fig. 8a), and 2) the total 2A25 volumetric rain in the inner core is greater than 5,000 mm $h^{-1}km^2$ (Fig. 8b). Secondly, for the range of conditionally mean rain rate < 7.5 mm h^{-1}, RI storms have higher 2A25 rain rate in the inner core than storms in other intensity change categories, while in the higher rain rate spectrum (≥ 9.5 mm h^{-1}), RI storms have lower conditionally mean rain rate in the inner core (Fig. 8c). Lastly, same as Fig. 4c, no necessary conditions for RI in terms of conditionally mean rain rate (Fig. 8c) in the inner core are found.

3.3 Lightning

TRMM observations within the TMI swath (similar swath width with LIS) are used in this section to compare lightning characteristics in the inner core, inner rainband, and outer rainband regions for different intensity change categories. Fig. 9a shows the percentage of TRMM TC overpasses with lightning in different TC regions and intensity change categories. For the inner core region with lightning, the percentage is the lowest for storms that will undergo RI and the highest for weakening storms. There are only about 7% of RI storms having lightning in the inner core, while the percentage is about 11-12% for storms in other intensity change categories. For the outer rainband region, the reverse relationship is seen. The percentage of overpasses with lightning in the outer rainband region is the highest for RI storms (37%), followed by storms in slowly intensifying (33%), neutral (25%), and weakening (20%) categories.

Fig. 9b shows the flash count per 2A12 raining area for inner core, inner rainband, and outer rainband regions of TCs in different storm intensity categories. After normalizing the flash counts by 2A12 raining area, lightning production in the inner core region is the lowest for storms that will undergo RI, second lowest for slowly intensifying storms, the third lowest for weakening storms, and the highest for neutral storms. The lightning density per raining area in the inner core for RI storms is more than a factor of 2 smaller than that for neutral and weakening storms. Generally it is seen that the lightning density per raining area in the inner core increases as the rate of intensification decreases. In the inner rainband region, the lightning density (per raining area) is the highest for neutral storms and the lowest for weakening storms, with RI and SI categories in between. In the outer rainband region, the order is almost the reverse as in the inner core region. The lightning density per raining area in the outer rainband region increases as the rate of intensity change increases. In the outer rainband region, storms that will undergo RI have the highest flash count per raining area, while storms that will weaken have the lowest flash density. Besides raining area, additional parameters, such as the 2A12 volumetric rain, the area of 85 GHz PCT < 250 K, and the area of 85 GHz PCT < 225 K, are used to normalize the flash counts. Similar to Fig. 9b, lightning density normalized by these additional parameters in the inner core (outer rainband) decreases (increases) as the rate of storm intensification increases (not shown).

4. Discussions

Results in section 3.1 and 3.2 indicate that RI storms do not necessarily have more extremely intense convection in the inner core than non-RI storms. Instead, a minimum threshold of convective intensity and total raining area and volumetric rain has to be achieved. This is consistent with the well-agreed observation by TC forecasters and researchers that the storm must be well-organized before intensifying and RI. As indicated by Fig. 2-8, the inner core region must be largely filled with at least moderate convection and moderate to heavy precipitation before RI. Some isolated asymmetric hot towers might exist and make contributions to the rapid intensification process in providing latent heating, but the necessary condition of RI is not those hot towers. As shown in Kieper and Jiang (2012), an early indicator of RI is the symmetric precipitative ring pattern around the storm center. Hot towers could be within the ring, but for most of the RI cases, the ring, which occurs 24 hours before RI, only contains shallow convection and warm rain. The findings in this study, along those in Kieper and Jiang (2012), support the notion that the azimuthally averaged latent heating release is much more important for the vortex intensification than asymmetric heating (e.g. Nolan et al. 2007).

Results in section 3.3 (Fig. 9) are consistent with DeMaria et al. (2012), which showed that lightning density in the inner core of rapidly weakening storms is larger than that for RI storms, and the lightning density in the rainband regions is higher for RI storms. DeMaria et al. (2012) tried to explain this behavior using the different interaction of inner core and rain band with the environmental shear. Our results in section 3.1 and 3.2 may help explain this from a different perspective. As shown above, the necessary condition for RI includes only moderate convective intensity and moderate to heavy rainfall in the inner core. In order to increase the likelihood of lightning, a fairly intense updraft is necessary to loft liquid droplets into the mixed phase region and to provide the supply of liquid hydrometeors, ice crystals, and graupel (Rakov and Uman 2003; Saunders 2008). The inner core region in RI storms is therefore not optimal to produce lightning. As hypothesized by DeMaria et al. (2012), the interaction of the environmental shear with the inner core PV is largely responsible for the relationships between TC intensity changes and lightning density. The environmental vertical shear can tilt the inner core PV and induce asymmetric intense convection, which is favorable for both lightning and short-term storm intensification. However, the negative effects of the vertical shear, and sometimes the downdrafts and cold pools from the enhanced convection halt the short term intensification.

On the other hand, the outer rainband region is outside of the core of high PV. As indicated by previous studies (Molinari et al. 1994, Houze 2010, DeMaria et al. 2012, JRC), the outer rainband region is similar to the background environment. The lightning density in that region is simply providing a measure whether or not the storm environment is favorable for atmospheric convection. The result in Fig. 9 supports the notion that for RI storms, the environment is more favorable for outer rainband convection than that for non-RI storms.

5. Conclusions

Using 11-yr TRMM passive microwave radiometer, infrared, radar, and lightning data, this study has statistically quantified convective and rainfall properties of tropical cyclones (TCs) for different storm intensity change categories. Four 24-h future intensity change categories are defined: rapidly intensifying (RI), slowly intensifying, neutral, and weakening. The storm inner core, inner rainband, and outer rainband regions were separated manually based on convective structures by a previous work presented in Jiang et al. (2012, JRC).

It is found that at weaker convective spectrum, RI storms have stronger ice scattering signature, higher cold cloud top, stronger radar reflectivity profile, and greater conditionally mean rain rate in the inner core than non-RI storms. However, at stronger convective spectrum, the convective intensity in the inner core of RI storms is not stronger than that for non-RI storms. Instead, the inner core of RI storms have the least percentage of pixels with 85 GHz PCT < 150 K (very strong convection, Fig. 3), the lowest conditionally mean rain rate in the higher rain rate spectrum (Fig. 4c and Fig. 8c), and the smallest near surface radar reflectivity at the 90%

percentile of radar reflectivity profile (Fig. 6). It is also found that RI storms always have larger raining area and total volumetric rain in the inner core.

All of these findings indicate that the maximum convective intensity in the inner core is not necessarily more intense prior to undergoing an RI episode than a slowly intensifying, neutral, or weakening episode. Instead, a minimum threshold of convective intensity, raining area, and total volumetric rain in the inner core has to be reached before a storm undergoes RI. The following necessary conditions of inner rainfall and convective properties are found for RI: maximum near surface radar reflectivity > 40 dBZ, maximum 20 (30, 40) dBZ echo height > 8 (6, 4) km, minimum 85 (37) GHz PCT < 235 (275) K, minimum IR T_{B11} < 220 K, total raining area > 3,000 km^2, and total volumetric rain > 5,000 mm h^{-1} km^2.

Above results are consistent with Jiang (2012), which demonstrated that extremely intense convection (i.e., hot towers) in the inner core increases the chance of RI, but the increase is not substantial. Similar to Kieper and Jiang (2012), this study supports the symmetric intensification mechanism proposed by previous studies, which showed that the axisymmtric latent heating release is more crucial for the vortex intensification than asymmetric heating (Ooyama 1969, Smith 1981, Shapiro and Willoughby 1982, Nolan et al. 2007).

The lightning analysis in this study has shown that the percentage of TRMM TC observations with lightning in the inner core decreases as the rate of storm intensification increases. The percentage is the lowest for storms that will undergo RI and the highest for weakening storms. However, for the outer rainband region, the reverse relationship is seen. The percentage of overpasses with lightning in the outer rainband region is the highest for RI storms (37%), followed by storms in slowly intensifying (33%), neutral (25%), and weakening (20%) categories. The lightning density (per unit raining area) shows the similar relationship to the storm intensification. Overall, total lightning activities in the inner core (outer rainband) have a negative (positive) relationship with storm intensification. This is consistent with DeMaria et al. (2012), which used an independent lightning dataset and showed similar relationships.

Acknowledgments

Thanks to Drs. Ed Zipser, Dan Cecil, and Steve Krueger for useful comments on this research and to Dr. Chuntao Liu for assistance with the TRMM PF database. Support for this study is provided by the NASA Precipitation Measurement Mission (PMM) grant, NASA New Investigator Program (NIP) grant, and NASA Hurricane Science Research Program (HSRP) grant. The authors thank Ramesh Kakar and Ming-Ying Wei (NASA headquarters) for their continued support of TRMM/PMM and hurricane sciences.

References

Cecil, D. J., and E. J. Zipser, 1999: Relationships between tropical cyclone intensity and satellite-based indicators of inner core convection: 85 GHz ice-scattering signature and lightning. *Mon. Wea. Rev.*, **127**, 103-123.

Cecil, D. J., E. J. Zipser, and S. W. Nesbitt, 2002: Reflectivity, ice scattering, and lightning characteristics of hurricane eyewalls and rainbands. Part I: Quantitative description. *Mon. Wea. Rev.*, **130**, 769-784.

DeMaria, M., R. DeMaria, J. Knaff, and D. Molenar, 2012: Tropical Cyclone Lightning and Rapid Intensity Change. *Mon. Wea. Rev*. doi:10.1175/MWR-D-11-00236.1, in press.

Gettelman, A., M. L. Salby, and F. Sassi (2002), Distribution and influence of convection in the tropical tropopause region, *J. Geophys. Res.*, **107(D10)**, 4080, doi:10.1029/2001JD001048.

Hall, T. J., and T. H. Vonder Haar (1999), The diurnal cycle of west Pacific deep convection and its relation to the special and temporal variations of tropical MCSs, *J. Atmos. Sci.*, **56**, 3401–3415.

Hendricks, E. A., M. T. Montgomery, and C. A. Davis, 2004: The role of "vortical" hot towers in the formation of tropical cyclone Diana (1984). *J. Atmos. Sci.*, **61**, 1209-1232.

Hendricks, E. A., M. S. Peng, B. Fu, and T. Li, 2010: Quantifying environmental control on tropical cyclone intensity change. *Mon. Wea. Rev.*, **138**, 3243-3271.

Houze Jr., R. A., 2010: Clouds in tropical cyclones. *Mon. Wea. Rev.*, **138**, 293-344.

Iguchi, T., T. Kozu, R. Meneghini, J. Awaka, and K. Okamoto, 2000: Rain-profiling algorithm for the TRMM Precipitation Radar. *J. Appl. Meteor.*, **39**, 2038–2052.

Jiang, H., C. Liu, E. J. Zipser, 2011: A TRMM-Based Tropical Cyclone Cloud and Precipitation Feature Database. *J. Appl. Meteor. Climatol.*, *50*, 1255-1274.

Jiang, H., 2012: The relationship between tropical cyclone rapid intensification and the strength of its convective precipitation features. *Mon. Wea. Rew.*, **140**, 1164-1176.

Jiang, H., E. M. Ramirez, and D. J. Cecil, 2012: Convective and rainfall properties of tropical cyclone inner cores and rainbands from 11 years of TRMM data. *Mon. Wea. Rev.*, in minor revision.

Kaplan, J., M. DeMaria, J. A. Knaff, 2010: A Revised Tropical Cyclone Rapid Intensification Index for the Atlantic and Eastern North Pacific Basins. *Wea. Forecasting*, **25**, 220–241.

Kelley, O. A., J. Stout, and J. B. Halverson, 2004: Tall precipitation cells in tropical cyclones eyewalls are associated with tropical cyclone intensification. *Geophys. Res. Lett.*, **31**, L24112, doi: 10.1029/2004GL021616.

Kelley O. A., J. Stout, J. B. Halverson, 2005: Hurricane intensification detected by continuously monitoring tall precipitation in the eyewall, *Geophys. Res. Lett*., **32**, L20819, doi: 10.1029/2005GL023583.

Kieper, M., and H. Jiang, 2012: Predicting tropical cyclone rapid intensification using the 37 GHz ring pattern identified from passive microwave measurements. *Geophys. Res. Lett.*, in press.

Kummerow, C., W. S. Olson, and L. Giglio, 1996: A simplified scheme for obtaining precipitation and vertical hydrometeor profiles from passive microwave sensors. *IEEE Transactions on Geosci. and Remote Sensing.* **34**, 1213-32

Lyons, W. A., and C. S. Keen, 1994: Observations of lightning in convective supercells within tropical storms and hurricanes. *Mon. Wea. Rev.*, **122**, 1897-1916.

Machado, L. A. T., W. B. Rossow, R. L. Guedes, A. W. Walker, 1998: Life Cycle Variations of Mesoscale Convective Systems over the Americas. *Mon. Wea. Rev.*, **126**, 1630–1654.

Mapes, B. E., and R. A. Houze, 1993: Cloud clusters and superclusters over the oceanic warm pool. *Mon. Wea. Rev.,* **121,** 1398–1416.

McGaughey, G., E. J. Zipser, R. W. Spencer, and R. E. Hood, 1996: High resolution passive microwave observations of convective systems over the tropical Pacific Ocean. *J. Appl. Meteor*., **35**, 1921-1947.

Merrill, R. T., 1988: Environmental influences on hurricane intensification. *J. Atmos. Sci.*, **45,** 1678-1687.

Mohr, K. I., and E. J. Zipser, 1996a: Defining mesoscale convective systems by their 85-GHz ice scattering signatures, *Bull. Amer. Meteor. Soc.*, **77**, 1179-1189.

Mohr, K. I., and E. J. Zipser, 1996b: Mesoscale convective systems defined by their 85-GHz ice scattering signature: Size and intensity comparison over tropical oceans and continents. *Mon. Wea. Rev.*, **124**, 2417-2437.

Molinari, J., P. K. Moore, V. P. Idone, R. W. Henderson, and A. B. Saljoughy, 1994: Cloud-to-ground lightning in Hurricane Andrew. *J. Geo- phys. Res.*, **99**, 16 665-16 676.

Molinari, J., P. K. Moore, and V. P. Idone, 1999. Convective structure of hurricanes as revealed by lightning locations. *Mon. Wea. Rev.*, **127**, 520-534.

Montgomery, M. T., M. E. Nicholls, T. A. Cram, and A. B. Saunders, 2006: A vortical hot tower route to tropical cyclogenesis. *J. Atmos. Sci.*, **63**, 355-386.

Montgomery, M. T., and R. K. Smith, 2011: Paradigms for tropical-cyclone intensification. *Q. J. R. Meteorol. Soc.* 137, 1–31.

Nolan, D. S., Y. Moon, and D. P. Stern, 2007: Tropical cyclone intensification from asymmetric convection: energetics and efficiency. *J. Atmos. Sci*., **64**, 3377–3405.

Ooyama, K., 1969: Numerical simulation of the life cycle of tropical cyclones. *J. Atmos. Sci*., **26**, 3–40.

Rakov, V. A., and M. A. Uman, 2003: Lightning: Physics and Effects. *Cambridge University Press*, 687 pp.

Rao, G. V. and P. D. MacArthur, 1994: The SSM/I estimated rainfall amounts of tropical cyclones and their potential in predicting the cyclone intensity changes. *Mon. Wea. Rev.*, **122**, 1568-1574.

Saunders, C., 2008: Charge separation mechanisms in clouds. *Space Sci. Rev.*, **137**, 335-353.

Shapiro, L. J., and H. E. Willoughby, 1982: The response of balanced hurricanes to local sources of heat and momentum. *J. Atmos. Sci.*, **39**, 378-394.

Smith, R. K., 1981: The cyclostrophic adjustment of vortices with application to tropical cyclone modification. *J. Atmos. Sci.*, **38**, 2021-2030.

Spencer, R. W., H. M. Goodman, and R. E. Hood, 1989: Precipitation retrieval over land and ocean with the SSM/I: Identification and characteristics of the scattering signal. *J. Atmos. Oceanic Technol*, **6**, 254–273.

Steranka J., E. B. Rodgers, and R. C. Gentry, 1986: The relationship between satellite measured convective bursts and tropical cyclone intensification. *Mon. Wea. Rev.*, **114**, 1539-1546.

Yuter, S. E., R. A. Houze, 1995: Three-Dimensional Kinematic and Microphysical Evolution of Florida Cumulonimbus. Part II: Frequency Distributions of Vertical Velocity, Reflectivity, and Differential Reflectivity. *Mon. Wea. Rev.*, **123**, 1941–1963.

Zuidema, P., 2003: Convective Clouds over the Bay of Bengal. *Mon. Wea. Rev.*, **131,** 780–798.

TABLES

Table 1. Definition of rapidly intensifying (RI), slowly intensifying (SI), netrual (N), and weakening (W) intensity change categories and respective TMI and PR observed TC overpasses. V_{max} and V_{max24} are the current (at the TRMM observation time) and future 24 h maximum wind speed intensity of the storm.

Intensity Change	Maximum Wind Speed Range [kts]	TMI TC overpasses	PR TC overpasses
RI	$v_{max24} - v_{max} \geq 30$	181	64
SI	$10 \leq v_{max24} - v_{max} < 30$	779	316
N	$-10 < v_{max24} - v_{max} < 10$	1183	490
W	$v_{max24} - v_{max} \leq -10$	569	230
Total		2712	1100

Table 2. The distribution of different intensity change samples as a function of different initial TC intensities, i.e., tropical depression (TD), tropical storm (TS), category 1-2 (CAT12) and 3-5 (CAT35) hurricanes for TMI and PR swath samples, respectively.

================ TMI swath ===========================

	TD	TS	CAT12	CAT35
RI	31	83	63	4
SI	312	306	114	47
N	502	395	184	102
W	8	188	215	158

================ PR swath ===========================

	TD	TS	CAT12	CAT35
RI	9	32	21	2
SI	127	120	48	21
N	200	166	86	38
W	4	73	87	66

Table 3. The distribution of different intensity change samples as a function of different TC basins, i.e., Atlantic (ATL), east central Pacific (EPA), northwest Pacific (NWP), north Indian Ocean (NIO), south Indian Ocean (SIO), and south Pacific (SPA) for TMI and PR swath samples, respectively.

======================== TMI swath ==========================

	ATL	EPA	NWP	NIO	SIO	SPA
RI	26	23	72	7	3	15
SI	137	91	291	36	160	64
N	239	211	322	53	276	82
W	96	127	166	15	113	52

======================== PR swath ==========================

	ATL	EPA	NWP	NIO	SIO	SPA
RI	11	6	30	0	12	5
SI	65	33	121	16	50	31
N	114	77	134	16	122	27
W	40	53	71	5	40	21

FIGURE CAPTIONS

Figure 1. Locations of TRMM (a) TMI and (b) PR swath TC overpasses used in this study.

Figure 2. Cumulative distribution functions (CDFs) of (a) minimum 85 GHz PCT [K] (b) minimum 37 GHz PCT [K], and (c) minimum T_{B11} [K] in the inner core of TCs in different intensity change stages.

Figure 3. CDFs of percentage of pixels with 85 GHz PCT < (a) 250 K, (b) 225 K, and (c) 150 K in the inner core of TCs in different intensity change stages.

Figure 4. CDFs of 2A12 (a) raining area, (b) volumetric rain, and (c) conditionally mean rain rate in the inner core of TCs in different intensity change stages.

Figure 5. Contoured frequency by altitude diagrams (CFADs) of maximum radar reflectivity in the inner core of TCs in (a) RI, (b) SI, (c) N, and (d) W intensity change stages. Bottom 10^{th} percentile (dash lines), median (solid lines), and 90^{th} percentile (dotted lines) of vertical profiles of maximum radar reflectivity are shown in each panel.

Figure 6. Bottom 10^{th} percentile (dash lines), median (solid lines), and 90^{th} percentile (dotted lines) of vertical profiles of maximum radar reflectivity in the inner core of TCs in different intensity change stages.

Figure 7. Box and whisker plots of 2A25 (a) maximum near surface radar reflectivity, (b) maximum height of 20 dBZ radar echo, (c) maximum height of 30 dBZ radar echo, and (d) maximum height of 40 dBZ radar echo in the inner core of TCs in different intensity change stages. The top of the box represents the 75% percentile, the center line the median, and the bottom of the box the 25% percentile. The whiskers extend to minimum and maximum of the range and outliers are plotted individually with circles.

Figure 8. CDFs of PR 2A25 (a) raining area, (b) volumetric rain, and (c) conditionally mean rain rate in the inner core of TCs in different intensity change stages.

Figure 9. Figure 9. (a) Percentage of TC overpasses with lightning and (b) flash count per 2A12 raining area in IC, IB, and OB regions of TCs in different intensity change stages.

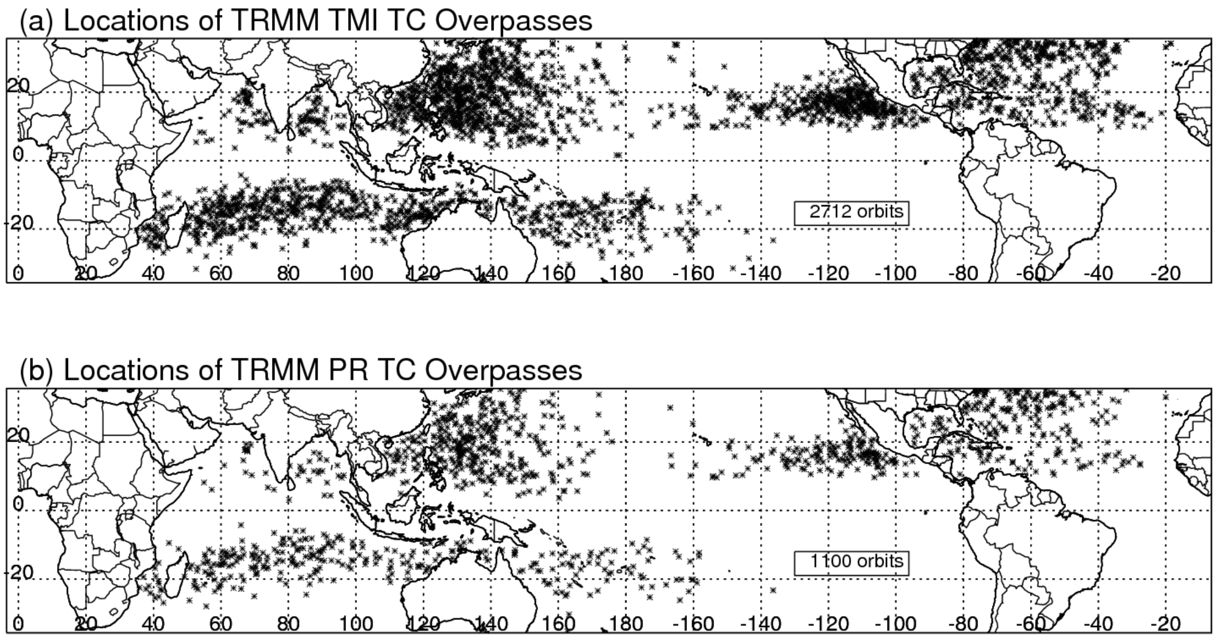

Figure 1. Locations of TRMM (a) TMI and (b) PR swath TC overpasses used in this study.

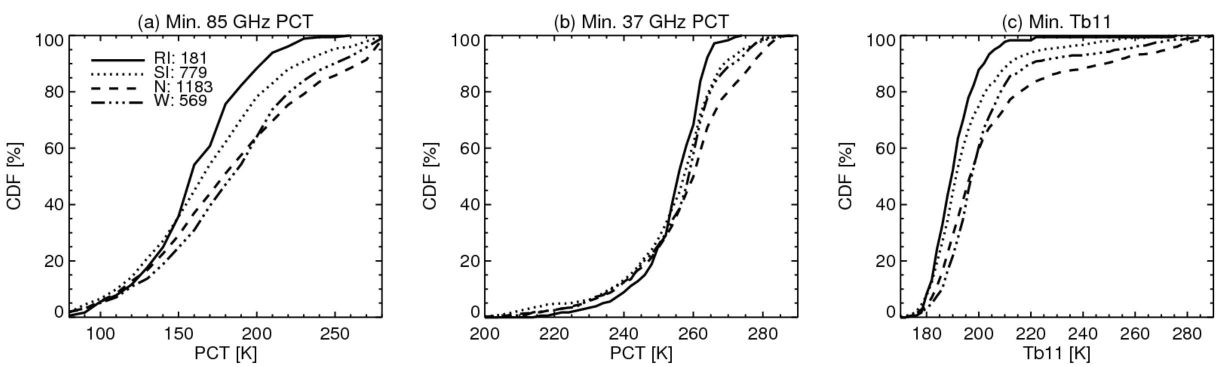

Figure 2. Cumulative distribution functions (CDFs) of (a) minimum 85 GHz PCT [K] (b) minimum 37 GHz PCT [K], and (c) minimum T_{B11} [K] in the inner core of TCs in different intensity change stages.

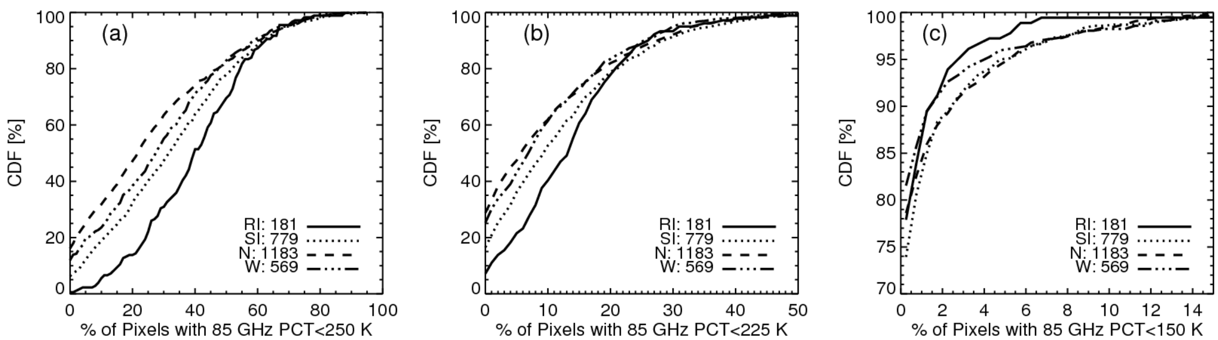

Figure 3. CDFs of percentage of pixels with 85 GHz PCT < (a) 250 K, (b) 225 K, and (c) 150 K in the inner core of TCs in different intensity change stages.

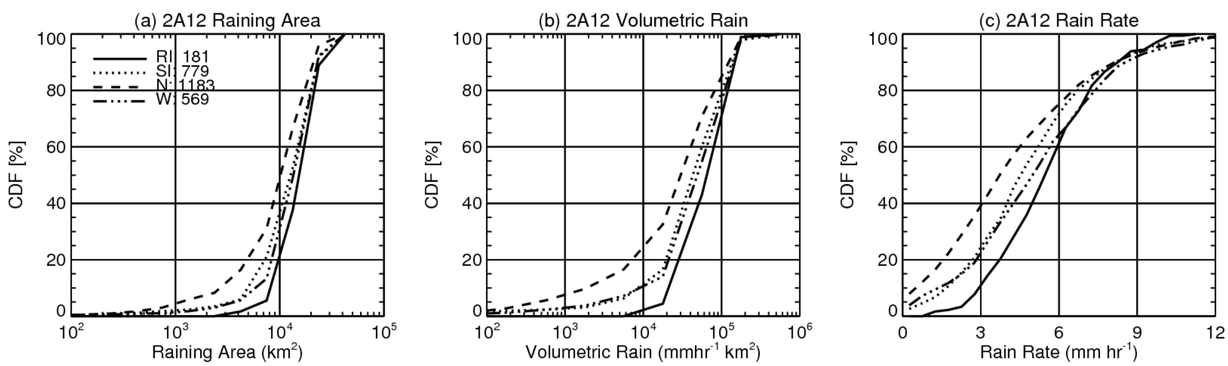

Figure 4. CDFs of 2A12 (a) raining area, (b) volumetric rain, and (c) conditionally mean rain rate in the inner core of TCs in different intensity change stages.

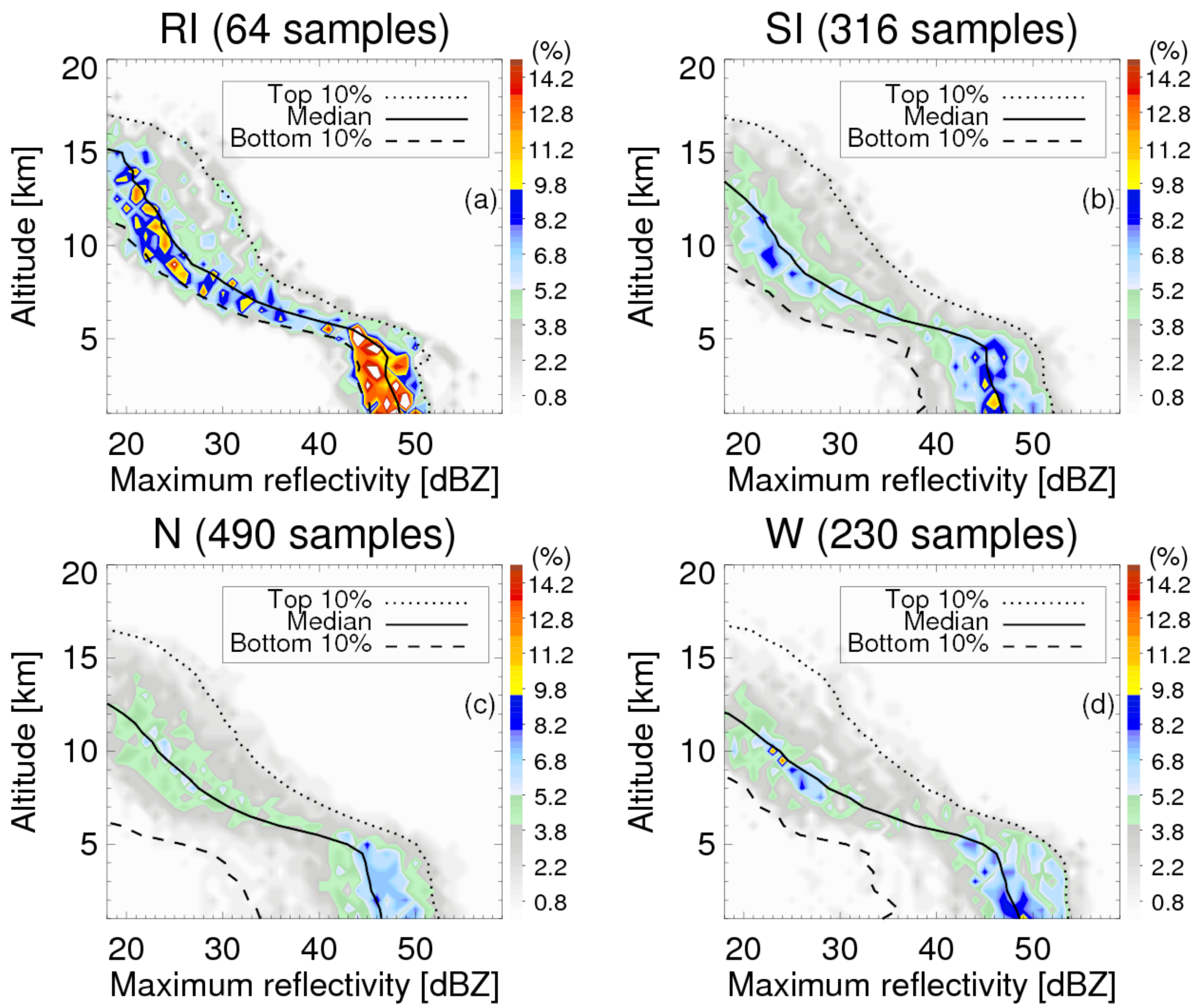

Figure 5. Contoured frequency by altitude diagrams (CFADs) of maximum radar reflectivity in the inner core of TCs in (a) RI, (b) SI, (c) N, and (d) W intensity change stages. Bottom 10th percentile (dash lines), median (solid lines), and 90th percentile (dotted lines) of vertical profiles of maximum radar reflectivity are shown in each panel.

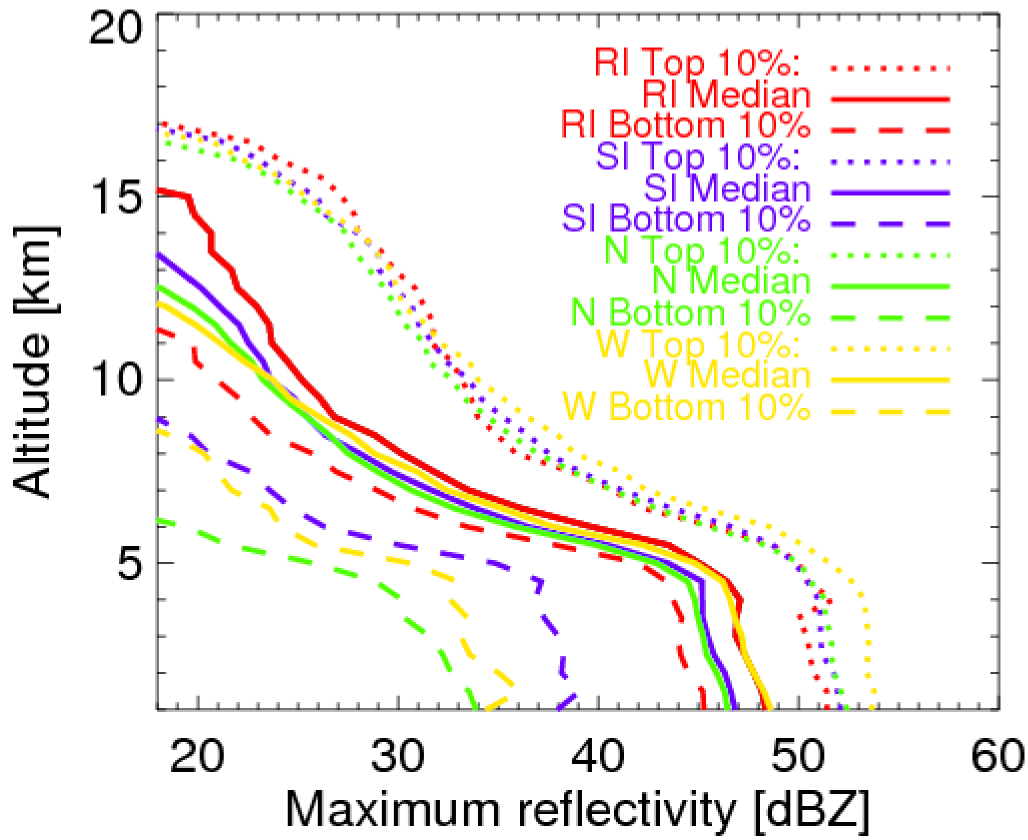

Figure 6. Bottom 10th percentile (dash lines), median (solid lines), and 90th percentile (dotted lines) of vertical profiles of maximum radar reflectivity in the inner core of TCs in different intensity change stages.

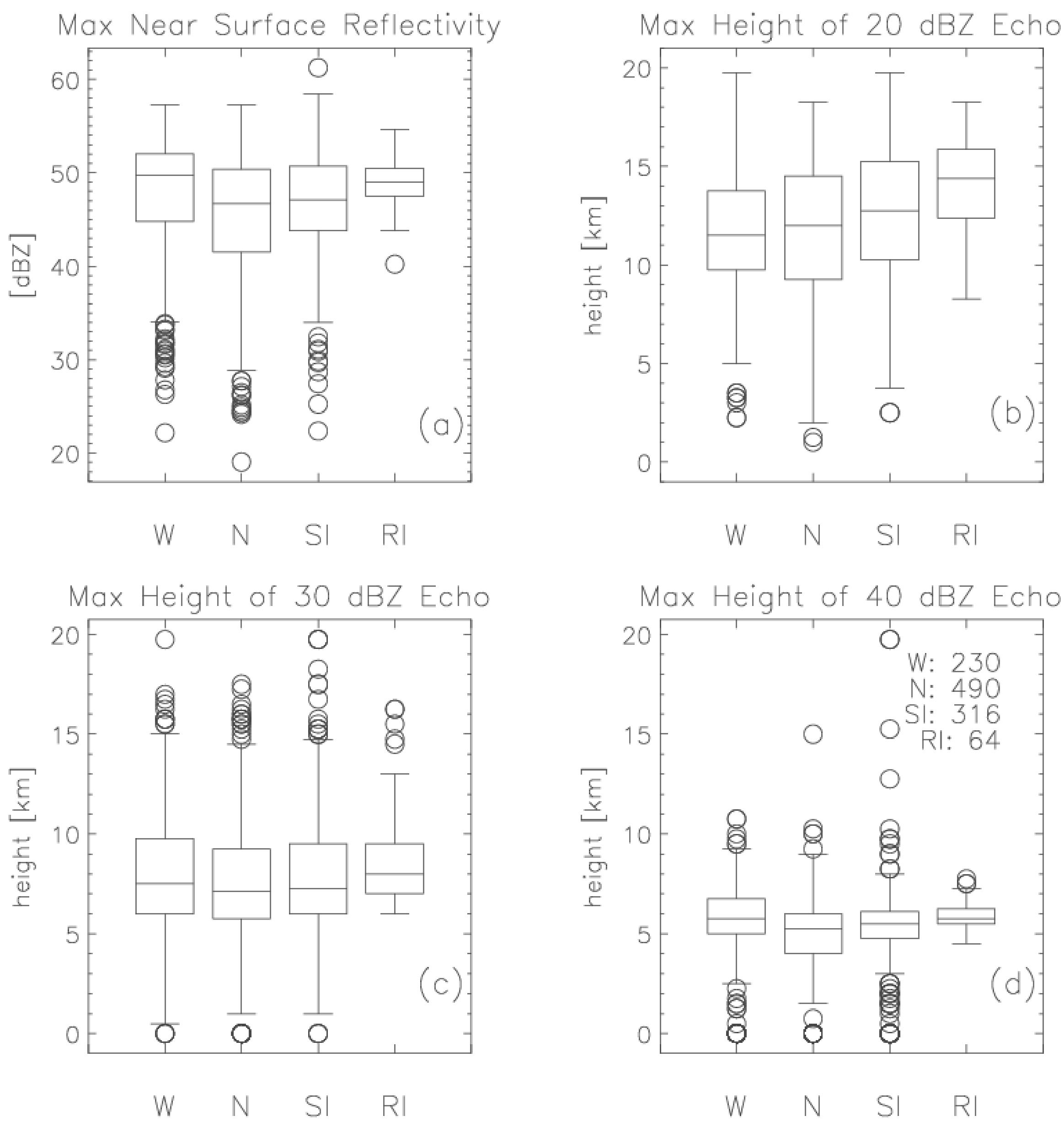

Figure 7. Box and whisker plots of 2A25 (a) maximum near surface radar reflectivity, (b) maximum height of 20 dBZ radar echo, (c) maximum height of 30 dBZ radar echo, and (d) maximum height of 40 dBZ radar echo in the inner core of TCs in different intensity change stages. The top of the box represents the 75% percentile, the center line the median, and the bottom of the box the 25% percentile. The whiskers extend to minimum and maximum of the range and outliers are plotted individually with circles.

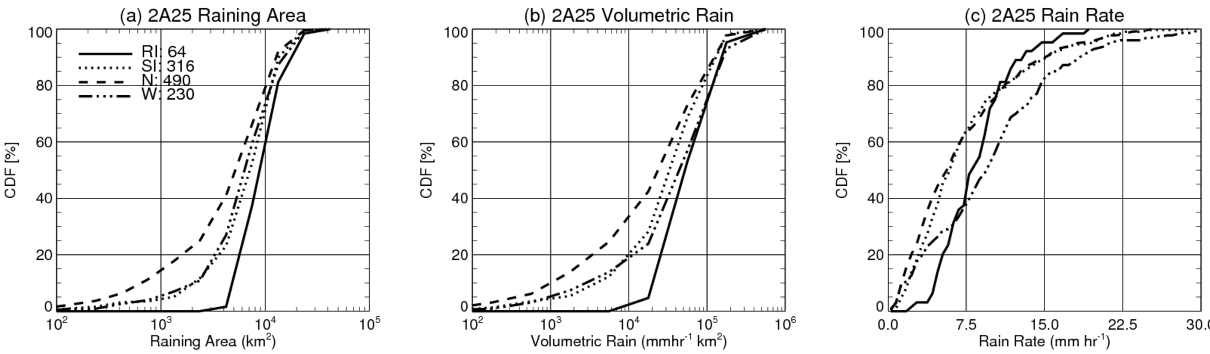

Figure 8. CDFs of PR 2A25 (a) raining area, (b) volumetric rain, and (c) conditionally mean rain rate in the inner core of TCs in different intensity change stages.

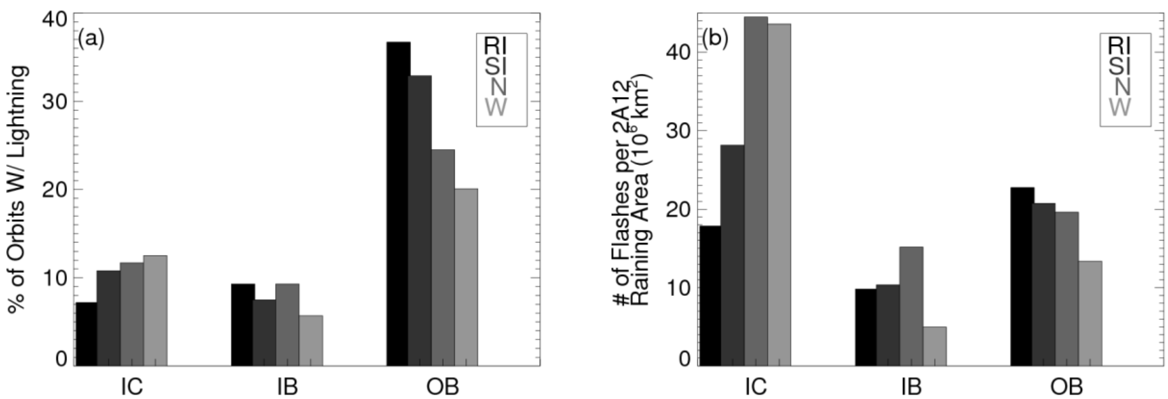

Figure 9. (a) Percentage of TC overpasses with lightning and (b) flash count per 2A12 raining area in IC, IB, and OB regions of TCs in different intensity change stages.